Published in "Physical Review E statistical, nonlinear, and soft matter physics
84(1): 016107, 2011"
which should be cited to refer to this work.

Concentration dependent refractive index of a binary mixture at high pressure

Fabrizio Croccolo,[1,a)] Marc-Alexandre Arnaud,[2] Didier Bégué,[2] and Henri Bataller[1,b)]
[1]*Laboratoire des Fluides Complexes - UMR 5150, Université de Pau et des Pays de l'Adour, BP 1155, 64013 Pau Cedex, France*
[2]*Institut Pluridisciplinaire de recherche sur l'Environnement et les Matériaux (IPREM) - UMR 5254, CNRS - Equipe de Chimie Physique, Université de Pau et des Pays de l'Adour, 2 avenue du Président Angot, 64053 Pau Cedex 9, France*

In the present work binary mixtures of varying concentrations of two miscible hydrocarbons, 1,2,3,4-tetrahydronaphtalene (THN) and n-dodecane (C12), are subjected to increasing pressure up to 50 MPa in order to investigate the dependence of the so-called concentration contrast factor (CF), i.e., $(\partial n/\partial c)_{p,T}$, on pressure level. The refractive index is measured by means of a Mach-Zehnder interferometer. The setup and experimental procedure are validated with different pure fluids in the same pressure range. The refractive index of the THN-C12 mixture is found to vary both over pressure and concentration, and the concentration CF is found to exponentially decrease as the pressure is increased. The measured values of the refractive index and the concentration CFs are compared with values obtained by two different theoretical predictions, the well-known Lorentz-Lorenz formula and an alternative one proposed by Looyenga. While the measured refractive indices agree very well with predictions given by Looyenga, the measured concentration CFs show deviations from the latter of the order of 6% and more than the double from the Lorentz-Lorenz predictions.

I. INTRODUCTION

A number of fluid properties and phenomena can be accurately and conveniently investigated by means of refined quantitative optical techniques which take advantage of the use of some, typically coherent, light source. Just to give some examples close to our experience: fluid properties like the mass diffusion coefficient of binary mixtures,[1] the Soret coefficient,[1–5] phenomena like non-equilibrium fluctuations[6–13] have been extensively studied through techniques such as Mach-Zehnder interferometry,[1] static and dynamic light scattering,[10,11,14–17] beam deflection,[2–5] shadowgraph[6,8–10,12,13] and other scattering in the near field (SINF) techniques.[11,12,18–21] In most of the aforementioned cases one needs to know *a priori* the dependence of the refractive index of the liquid under analysis on the relevant parameter (concentration, temperature, etc.) in order to derive accurate measurements. This dependence is also commonly referred to as the contrast factor (CF) defined as $(\partial n/\partial c)_{p,T}$ for the concentration CF and $(\partial n/\partial T)_{p,c}$ for the temperature CF. Unfortunately, literature data are not always available for the mixture of interest, and when available, they are not always of good quality as pointed out previously.[22,23] Moreover, data are typically limited to atmospheric pressure, and theoretical predictions are not always reliable in many practical cases.

Recently, the oil industry has shown great interest in studying transport properties.[24] Since conditions under which crude oil is found underground imply high pressure (HP) and diffusion in porous media, it is important to analyze the influence of the pressure and the interaction with a porous medium on the transport properties of liquid mixtures.[25] This is done to achieve better reliability of the algorithms used for simulating the crude oil behavior in oil fields. Nevertheless, thermal diffusion data under reservoir conditions are very scarce and not very recent.[26,27] In this view, we are interested in performing high-pressure interferometric measurements on binary mixtures stressed by a temperature gradient and going through Soret separation across a porous medium. For doing this we first attempted to precisely measure the concentration CF of a binary mixture in a wide pressure range. As a consequence we had the need to validate our experimental values with a theoretical approach able to account for the effect of pressure.

The choice of the particular model binary mixture to study has been mainly driven by the need of having a mixture which is already well characterized at atmospheric pressure,[28] and which also provides a strong Soret effect. On this basis the liquid mixture has been chosen as 1,2,3,4-tetrahydronaphtalene (THN)–n-dodecane (n-C12) kept at a constant temperature $T_{\text{mean}} = 25\,^{\circ}\text{C}$.

The remainder of this paper is organized as follows: in Sec. II, the experimental setup is described along with details of the high pressure thermodiffusion cell and the interferometric setup; in Sec. III, details are provided for the algorithm that allows us to obtain the refractive index as a function of the pressure and for the procedure to obtain the refractive

a)Present address: Physics Department, University of Fribourg, Ch. Du Musée 3, CH-1700 Fribourg, Switzerland.
b)Electronic mail: henri.bataller@univ-pau.fr.

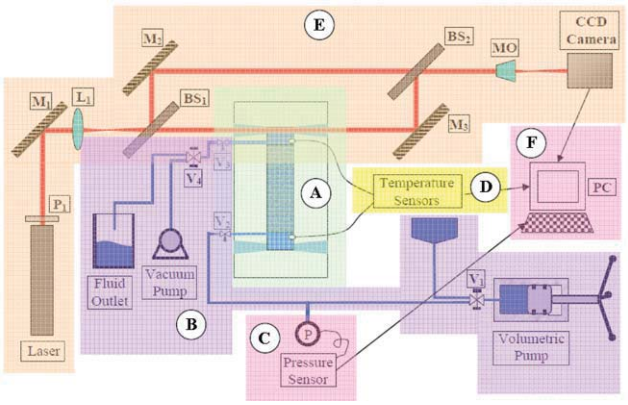

FIG. 1. Experimental set-up including: (A) high pressure cell without porous media inside, (B) filling and high pressure system, (C) pressure measurement, (D) temperature measurement, (E) Mach-Zehnder interferometer, and (F) control hardware and software.

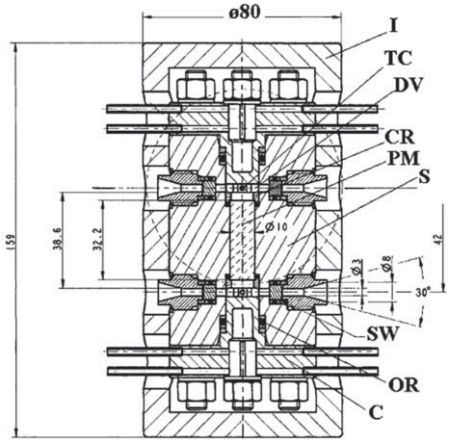

FIG. 2. High pressure cell: (C) cap filled with water; (OR) O-ring; (SW) sapphire window; (S) steel; (PM) porous media; (CR) centering ring; (DV) dead volume; (TC) thermocouple; and (I) insulator.

index derivative $(\partial n/\partial c)_{p,T}$; in Sec. IV, experimental results are presented and compared with theory; and finally several conclusions are provided in Sec. V.

II. EXPERIMENTAL SET-UP

The core of the experimental apparatus is a high pressure cell, specifically designed for performing thermodiffusion experiments at high pressure and across a porous medium. In Fig. 1 the whole apparatus is sketched to summarize the functional elements, consisting of

(A) high pressure cell;
(B) filling and high pressure system;
(C) pressure measurement;
(D) temperature measurement;
(E) Mach-Zehnder interferometer;
(F) control hardware and software.

A. High pressure cell

The design of the high pressure cell has been optimized for performing interferometric measurements at high pressure for a liquid mixture under a temperature gradient and filling a porous medium. The high pressure cell consists of a stainless steel cylinder with two liquid circuits at its top and bottom. Pure water circulating through these loops comes from two distinct temperature controlled baths to keep the top and bottom of the cell at two distinct temperatures with a stability of $\pm 0.1\,^{\circ}$C over many days. Figure 2 shows the detail of the cell. The interior of the cell has a volume $V = 3.5$ ml with a height $h = 45$ mm. Its central part has a cylindrical shape whose diameter is $d = 10$ mm. Most of this volume is normally filled by a porous medium consisting of a monolithic silica cylinder of the same diameter of the cell interior and height $h' = 32.2$ mm. The porous medium is essential for our studies in which we attempt to mimic the behavior of fluids within oil fields. In fact, typical oil fields conditions are that of fluids moving through porous media at high pressure and with temperature gradients. The porous media also helps to avoid convection in the cell. At the two extremities of the porous medium, two free volumes which we refer to as dead volumes (DVs) allow refractive index measurements by means of interferometry. The optical access to the two DVs is provided by two opposing sapphire windows for each DV letting a laser beam pass through the fluid perpendicular to the cell axis. Figure 3 shows the detail of one DV. As it can be seen, the DV has a "T" shape. As explained in Sec. IV, the value of the optical path has been obtained from the analysis of experimental data taken with pure toluene, hexane, and water, and it is $d^* = 21.5 \pm 0.3$ mm. The cell is designed to maintain a liquid mixture in a pressure range between 1 and 1000 bar and in a temperature range between 5 °C and 40 °C. The cell is externally covered by a ceramic insulator in order to limit heat transfer between the cell walls and the environment. Since the experiments we report in this work have been performed in isothermal conditions and influence due to the porous medium was to be avoided, the latter has been removed from the cell before starting the experiment campaign.

B. Filling and high pressure system

The cell is filled by connecting it to a filling system consisting of: a rotary vacuum pump able to evacuate most of the air from the cell before filling operations down to a residual pressure of about 10 Pa; a fluid vessel at atmospheric pressure; a manual volumetric pump, and a number of valves to

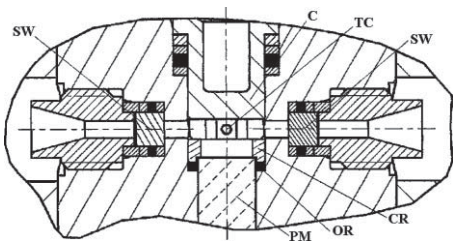

FIG. 3. Detail of the dead volume in the cell: (PM) upper part of the porous media; (OR) O-ring; (CR) centering ring; (SW) sapphire window; (TC) thermocouple; and (C) cap filled with water.

facilitate the procedure. Briefly, after a low vacuum is made inside the cell, the mixture to be studied is transferred to the cell by letting it enter from its bottom side. In this phase, visual inspection through the sapphire windows is needed to check bubble presence. The cell is then abundantly fluxed with the fluid mixture. At the end of the procedure the valve V_4 is closed and the volumetric pump is operated to modify the liquid pressure within the cell and perform the experimental runs.

C. Pressure measurement

A manometer (Keller, PAA-33X/80794, pressure range: $0.1 \div 100$ MPa, precision ± 0.03 MPa) is connected between the volumetric pump and the cell and constantly checks the pressure of the fluid mixture. The manometer signal is transferred using an acquisition card (National Instruments, NI 9215) interfaced to a computer in order to save pressure data in synchrony with optical measurements.

D. Temperature measurement

At the top and bottom of the cell, two K-type thermocouples are positioned within the two DVs in contact with the liquid. Also the thermocouples are connected to the computer to save synchronized data. The connections between the electronics and the acquisition card needed separate and accurate grounding to limit the level of periodic noise in the temperature measurements.

E. Mach-Zehnder interferometer

The optical setup for the Mach-Zehnder interferometer is shown in Fig. 1. An He-Ne laser (Melles Griot, 25 LHP 151-230) operating with a wavelength of $\lambda = 632.8$ nm and a power of $P = 15$ mW generates a TEM_{00} plane wave which is used as is without further spatial filtering. The beam intensity is modulated by rotating a linear polarizer P_1 in front of the laser tube before performing each experiment. The beam is deflected by a metallic mirror M_1 and is made to diverge by means of a positive lens L_1 ($f = 2$ cm). A 50/50 beam splitter BS_1 divides the beam into two beams of equal intensity, the former passing through one DV of the cell (and then bent again by mirror M_3), while the latter is deflected by mirror M_2. The beams are recombined at a second 50/50 beam splitter BS_2 and eventually propagate to the CCD camera (Cohu, 7712-3000, 8-bit camera) after being captured by a microscope objective MO ($f = 2$ mm, 4X) placed at a distance $L = 15$ cm from the sensor plane. It has been chosen to investigate just one vertical line out of the entire image, because this is enough for a good characterization of the sinusoidal intensity modulation. The intensity of the laser and the exposure time of the CCD camera are tuned to prevent saturation of the CCD.

In the typical configuration for performing thermodiffusion experiments, the two cell DVs are within the two arms of the interferometer, thus allowing recovery of the refractive index differences between the two DVs. However, since in the present work the cell is isothermal and no concentration gradient is supposed to be present in the fluid mixture, only one DV is crossed by one interferometer arm, the other beam passing through air. In this way the variations of the refractive index of the fluid inside the cell are measured over time.

The entire optical set-up is mounted on an optical table, extensive tests have been performed to evaluate the effect of environmental vibrations on the quality of the interferometric measurements and different actions have been taken to reduce the noise, mainly provided by the thermostatic baths operating very close to the optical table. These actions led to a satisfactory reduction of high frequency noise such that the RMS noise afterwards was on the order of 0.1 fringes over 24 h.

III. EXPERIMENTAL PROCEDURE

The aim of the interferometric measurements is to get quantitative information about the phase difference between the two laser beams at the interference plane which is conjugated to the sensor plane by the microscope objective. Since one of the two beams passes through the cell while the other one is a reference beam passing in air, the interferogram phase that is acquired by the CCD camera changes as a function of the refractive index variation inside the cell. The phase difference at the interference plane can be written as

$$\vartheta = -(k_l - k_o) \cdot d^* = -\frac{2\pi}{\lambda_o}(n_l - n_o) \cdot d^*, \qquad (1)$$

where k_l is the wave vector of the laser beam passing through a length d^* of the liquid with refractive index n_l, k_o is the wave vector of both beams in air, and λ_o is the wavelength of the laser beam in vacuum. To obtain the desired information one has to identify the phase change in the recorded interference fringe pattern.

To achieve this, the pixel intensities over one vertical line (perpendicular to the fringe pattern) are fit with the following function via custom LABVIEW® software:

$$I(y) = a \cdot \cos^2(b \cdot y - c') + d. \qquad (2)$$

In Eq. (2) the quantity of interest is the phase term c', the other three terms being not expected to change too much during the experiment execution, as we checked by analyzing the fitting outputs. In order to improve the fitting results, the data are first normalized before feeding the fit procedure. The normalization aims at providing a uniform height to the sinusoidal function, which is not the case for the raw data because of beam non-uniformity and imperfect overlap of the two interfering beams, both caused by defects of the optical elements.

The fitting software takes the output values of each fitting sequence as the initial values for the following one, thus actually performing automatic unwrapping of the phase. This means that the obtained phase values c' are not limited to the range $[-\pi/2, \pi/2]$ and do not need further unwrapping. In Fig. 4, a plot of the normalized pixel values as a function of the spatial position over the vertical line is plotted along with the fitting curve. Data points shown in Fig. 4 have also been averaged along the horizontal axis thus providing a consistent noise reduction. This procedure, however, does not

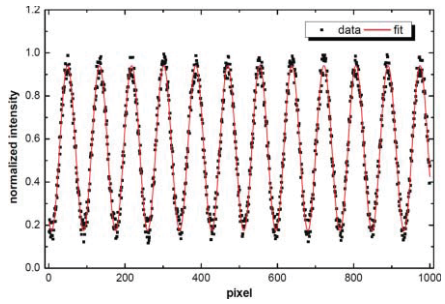

FIG. 4. Normalized values of interference intensities as recorded by the CCD camera as a function of the vertical position after averaging over horizontal lines (black square dots) and values for fitting function (red continuous line).

significantly increase the quality of the fitting, for this reason all the analyses in the following have been performed by fitting data points of one single line, thus reducing the amount of resources needed for performing the fitting live.

The experimental procedure begins by introducing the given sample mixture (at one concentration value) into the cell with the procedure described in Sec. II, after which the cell is pressurized up to approximately 10 MPa. The pressure is manually changed at increments of 2.5 MPa using the volumetric pump from atmospheric pressure until 40 MPa and by increments of 1 MPa until 50 MPa. First the pressure is increased and then it is decreased over the same range. While the pressure is manually increased the software acquires an image every 100 ms and extracts in real-time one vertical line, previously chosen upon visual inspection of the interferograms, on which the fitting procedure is performed. The temperatures of the top and bottom DVs are also acquired together with the pressure within the cell. For each pressure slot a text file is saved containing the values of time, pressure, temperatures and phase as obtained by the fitting procedure. The pressure and the scrolled fringes as a function of time are shown for one pressure slot in Fig. 5. Noise in the pressure measurement is due to the somewhat low precision of the pressure sensor.

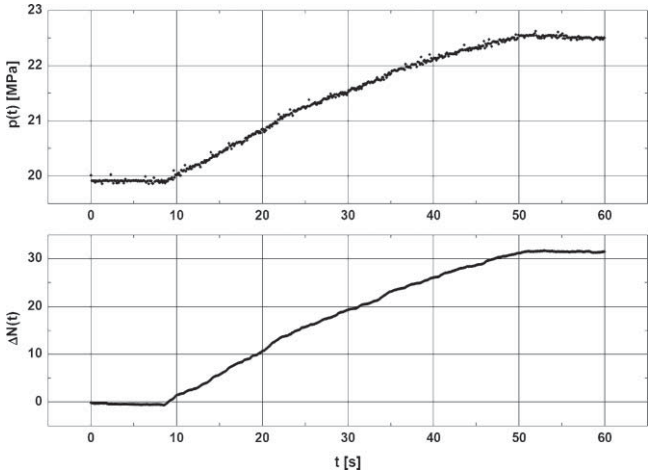

FIG. 5. The upper figure shows the pressure $p\,(t)$ and the lower figure shows the number of scrolled fringes $\Delta N\,(t)$ as a function of time t during the pressure increase from 20 and 22.5 MPa for the 50 wt.% binary mixture.

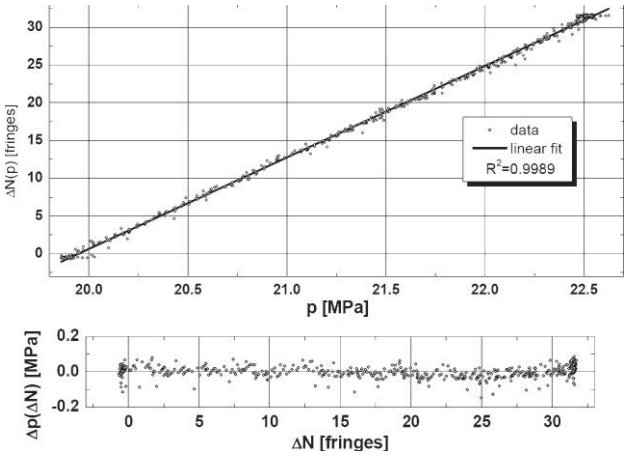

FIG. 6. The upper figure shows the number of scrolled fringes $\Delta N\,(p)$ as a function of pressure p for the same slot as Fig. 5, together with a linear fit. The lower figure shows the deviation of the pressure from the linear fit Δp as a function of the scrolled fringes ΔN.

In all measurements the phase variation as a function of pressure is always close to about one scrolled fringe per 0.1 MPa of pressure change within the cell. This poses a limit in the speed at which the pressure is changed during the experiment. We roughly limited the speed to less than 0.1 MPa/s, thus being sure to observe at least 10 recordings for each fringe scroll, sufficient to be sure not to lose fringes from the phase computation. During the pressure change, constant visual checks of the intensity profile and the fitting (as in Fig. 4) were also performed to be sure that the fitting procedure did not fail. There were few instances of fitting failures and the corresponding datasets were discarded and the corresponding measurements repeated.

To obtain the value of the variation of the phase as a function of the pressure, a linear fit was applied to the resulting data of fringe scrolling versus pressure for each pressure slot, as shown in Fig. 6.

As can be noticed by inspection of Figs. 5 and 6, the pressure values close to the extremities of the pressure slot consist of many data points because the recording is started some seconds before the pressure increase is initiated and stopped somewhat after its end. To avoid these points weighting too much in the fitting procedure, their frequency was calculated and its square inverse was used as a weight for the linear fit. Figure 6 also shows the deviation of the pressure from the values of the linear fit as a function of the scrolled fringes. From this representation one can notice that the pressure measurements are randomly scattered around the linear fit behavior with an RMS of 0.03 MPa. From the resulting $\Delta N/\Delta p$ fit one can obtain the refractive index of the mixture at different pressure levels through the following relation:

$$n\,(p_b) = n\,(p_a) + \frac{\lambda}{d^*} \cdot \frac{\Delta N}{\Delta p}\,(p_b - p_a)\,, \qquad (3)$$

where p_b is the final pressure, p_a the initial pressure in a slot, and the refractive index values at atmospheric pressure were taken from literature.

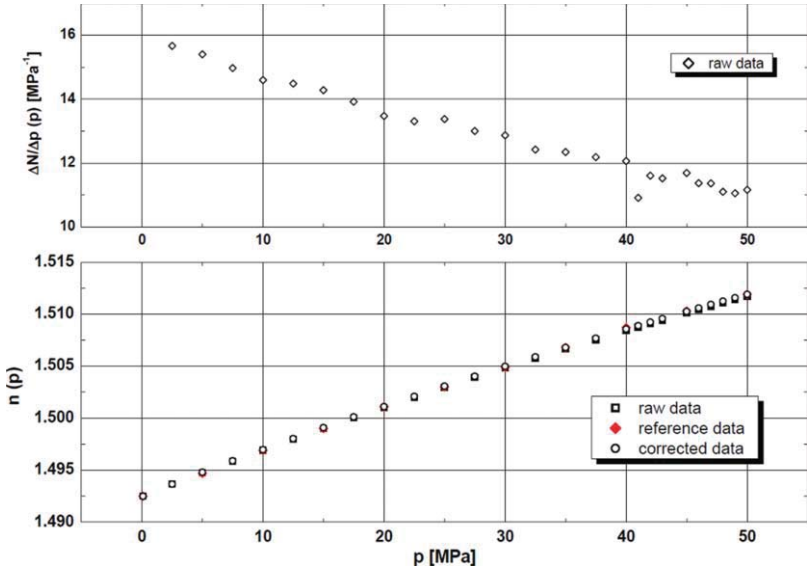

FIG. 7. The upper figure shows the number of scrolled fringes per MPa of pressure change $\Delta N/\Delta p\,(p)$ as a function of pressure p for pure toluene at 20 °C. The lower figure shows measured (□), reference values from literature (Ref. 29) (♦) and corrected (□) refractive index $n\,(p)$ as a function of pressure p.

Before starting the experimental runs with the binary system, we performed calibration measurements with toluene, hexane, and water.

IV. RESULTS AND DISCUSSION

A. Validation of the experimental procedure

In order to validate the high pressure cell and the measurement technique, we measured the refractive index of three different pure fluids (toluene, hexane, and water, which refractive indices as a function of pressure are given in literature[29–31]) as a function of pressure in the range from atmospheric pressure up to 50 MPa. In Fig. 7, we report the values of $\Delta N/\Delta p$ as a function of pressure for pure toluene at 20 °C, together with the refractive index as a function of pressure as recovered by using Eq. (3).

As suggested by Takagi *et al.*[29] as the pressure is increased the measurement of $\Delta N/\Delta p$ is overestimated and this can be taken into account by including a correction factor into Eq. (3). Including this correction, Eq. (3) can be written as

$$n\,(p_b) = n\,(p_a) + \frac{\lambda}{d^*} \cdot \left(\frac{\Delta N}{\Delta p} - \xi\,(p) \right) (p_b - p_a)\,, \qquad (4)$$

where $\xi(p)$ is the correction term for the strain on the optical windows due to pressure. Moreover, the determination of the refractive index is very much sensitive to the value of the optical path d^*. Therefore, aiming at calibrating our procedure, we proceeded in fitting our data to the reference values by using $\xi\,(p)$ and d^* as two fitting parameters. Following Takagi we use a linear equation for the correction term: $\xi\,(p) = ap + b$, but the first order term is typically much smaller than the constant one, so that we decided to neglect it and fit our data with the simpler function $\xi\,(p) = b$.

After fitting the data for all the three pure fluids the resulting optical path was $d^* = 21.5 \pm 0.3$ mm, the uncertainty being given by the deviation from the mean value, while our reference value from the cell provider was $d^* = 21.5 \pm 0.3$ mm. Also, the correction factor was $\xi\,(p) = 0.21 \pm 0.05$ MPa^{-1}.

In Fig. 8 we report the deviation of the toluene measurements from reference values at 20 and 30 °C, with and without the correction factor.

With the correction described above, the deviation of the corrected data from reference values has an RMS of about 5×10^{-5} and is randomly distributed around zero. Similar graphs and deviations were obtained for hexane and water. It is worth pointing out that this correction affects only the absolute determination of the refractive index, but does not affect the measurement of the concentration CF, since the latter is calculated as a derivative of values at different concentrations, but at the same pressure.

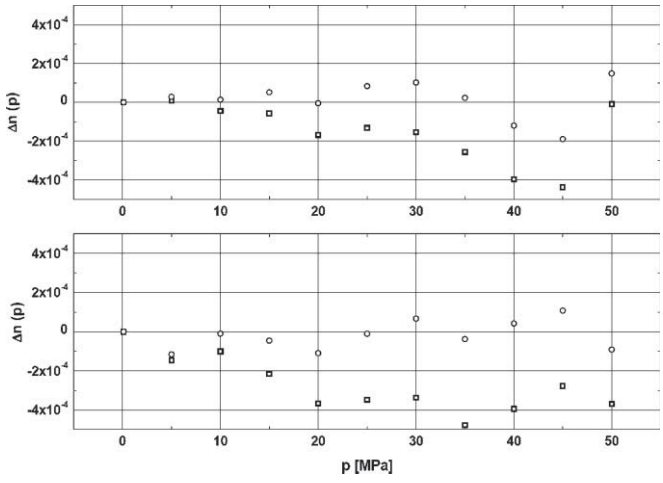

FIG. 8. Refractive index deviation from reference data (Ref. 29) for the measured values (□) and corrected with Eq. (4) measurements (○) as a function of the pressure p for the toluene at 20 °C in the upper figure and 30 °C in the lower figure.

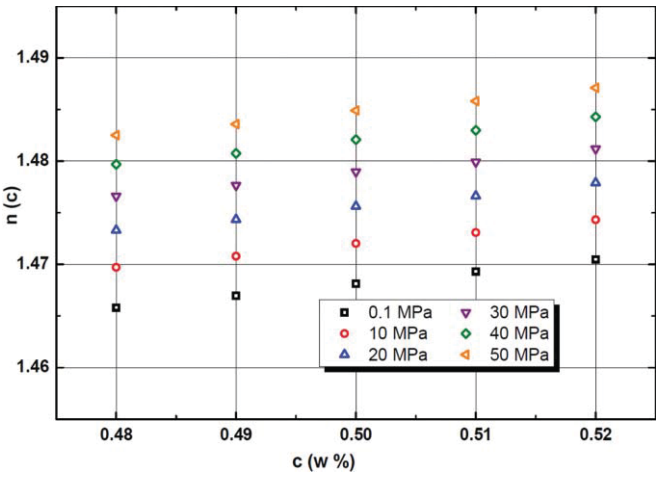

FIG. 9. Refractive index $n(c)$ of the THN + C12 mixture as a function of the concentration c, and for different pressure levels ranging from 0.1 up to 50 MPa.

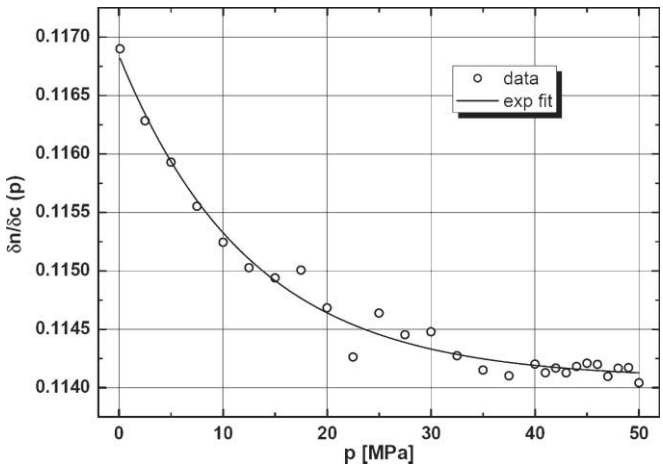

FIG. 10. Concentration CF for the mixture THN + C12 at 25 °C as a function of the pressure. Open circles represent experimental data points, while the continuous line is an exponential decay fit.

B. Measurements with the binary system

Sample mixtures of 1,2,3,4-tetrahydronaphtalene (THN) and n-dodecane (C12) are prepared at different concentrations ranging from 48 up to 52 wt.%, by preparing 100 g of solution. The balance sensitivity is on the order of 10^{-3} g, the uncertainty on c is thus estimated to be $\pm 1 \times 10^{-4}$.

The atmospheric values for the refractive index of the mixture are obtained by the empirical formula:[32]

$$n(c) = 1.418 + 0.0836c + 0.0333c^2, \tag{5}$$

which is valid for the THN + C12 mixture for all concentrations and at 25 °C. After introducing the samples and waiting for temperature equilibrium, we start the recording of the number of scrolled fringes per MPa. The refractive index is recursively calculated for all the pressure values up to 50 MPa as in Sec. III. The uncertainty on n is estimated at ± 0.00001 at 2.5 MPa and ± 0.0001 at 50 MPa.

In Fig. 9, the refractive index is shown as a function of the concentration of the THN + C12 mixture for different pressure levels: for the sake of clarity not all pressure values are shown.

The concentration CF is then given by $\mathrm{CF}(c_o) = \partial n/\partial c\,(c_o)|_{p,T}$. A linear fit was performed on the experimental values of $n(c)$, the slope of which is assumed to be equal to the concentration CF at $c_o = 0.5 = 50$ wt.%. Figure 10 shows the calculated concentration CF as a function of pressure.

The solid curve in Fig. 10 corresponds to an exponential decay fit, the equation of which is:

$$\frac{\partial n}{\partial c} = 0.1141 + 0.0027 \exp\left(-\frac{p}{12.6}\right). \tag{6}$$

From this we can deduce some qualitative information about the concentration contrast factor behavior as a function of pressure. First, the contrast factor is always positive, meaning that an increase of the refractive index is obtained if the mixture is enriched in THN whatever the pressure, as at atmospheric pressure. Second, there is a decrease of the value of the concentration contrast factor as pressure increases, meaning that the same variation of the concentration of the mixture gives rise to a smaller variation of its refractive index at high pressure. Third, the exponential decay shows a high pressure limit of 0.1141 which differs from the atmospheric pressure value of 0.1169 by about 3%.

C. Discussion

1. Working equations

The refractive index of a fluid can be theoretically predicted by the well-known Lorentz-Lorenz (LL) formula:[22,33]

$$\left[\frac{n^2-1}{n^2+2}\right]_{(\mathrm{LL})} = \frac{4\pi}{3} N_A \rho \frac{\alpha}{M}, \tag{7}$$

in which N_A is Avogadro's number, ρ the density of the fluid, M the molar mass, and α the molecular polarizability of the component. There exist different variants of the LL formula, among which the Looyenga (LO) approach provides the following result:[22,34]

$$[n^{2/3} - 1]_{(\mathrm{LO})} = \frac{4\pi}{3} N_A \rho \frac{\alpha}{M}. \tag{8}$$

Both these equations can be extended to fluid mixtures once a suitable mixing rule is provided. As a first and simple attempt, we will use a linear additive mixing rule so that the two formulas are extended to mixtures as follows:[22]

$$\left[\frac{n^2-1}{n^2+2}\right]_{(\mathrm{LL})} = \frac{4\pi}{3} N_A \rho \sum_i \frac{c_i \alpha_i}{M_i}, \tag{9}$$

$$[n^{2/3} - 1]_{(\mathrm{LO})} = \frac{4\pi}{3} N_A \rho \sum_i \frac{c_i \alpha_i}{M_i}, \tag{10}$$

in which c_i is the mass fraction, M_i the molar mass, and α_i the molecular polarizability of component i.

The concentration CF for a binary mixture with a linear mixing rule can be deduced to be

$$\left(\frac{\partial n}{\partial c}\right)_{p,T(\mathrm{LL})} = \frac{(n^2-1)(n^2+2)}{6n} \times \left[\frac{1}{\rho}\left(\frac{\partial \rho}{\partial c}\right)_{P,T} + \frac{\frac{\alpha_1}{M_1}-\frac{\alpha_2}{M_2}}{\frac{c\alpha_1}{M_1}+\frac{(1-c)\alpha_2}{M_2}}\right], \quad (11)$$

$$\left(\frac{\partial n}{\partial c}\right)_{p,T(\mathrm{LO})} = \frac{3}{2}(n-n^{1/3}) \times \left[\frac{1}{\rho}\left(\frac{\partial \rho}{\partial c}\right)_{P,T} + \frac{\frac{\alpha_1}{M_1}-\frac{\alpha_2}{M_2}}{\frac{c\alpha_1}{M_1}+\frac{(1-c)\alpha_2}{M_2}}\right], \quad (12)$$

in which $1/\rho\,(\partial\rho/\partial c)_{P,T} = \beta$ is the mass expansion coefficient of the mixture.

Two kind of comparison can be performed to validate our measurements. First, one can compare the left hands of Eqs. (9) and (10) (with the experimental values of n) with the corresponding right hands of the respective equations, in order to check the measured values of the refractive index n against the two different theoretical approaches. Second, one can compare the left hands of Eqs. (11) and (12) (with the measured values of the concentration CF) against the right hands of the same formulas. In this way, a check of the concentration CF against the two theories is obtained. In order to perform these comparisons one needs to know the values of the molecular polarizability of the two molecules as well as the density and the mass expansion coefficient of the mixture as a function of the pressure. While the latter have been measured by some of us in a previous experiment,[35] the former is not easy to measure and there exist no reference value in literature for the two components of choice at high pressure.

In order to obtain the polarizability, quantum calculations have been performed as detailed in the Appendix. Essentially these calculations showed a marginal dependence of the molecular polarizability upon pressure change and provided the values to be used in Eqs. (9)–(12).

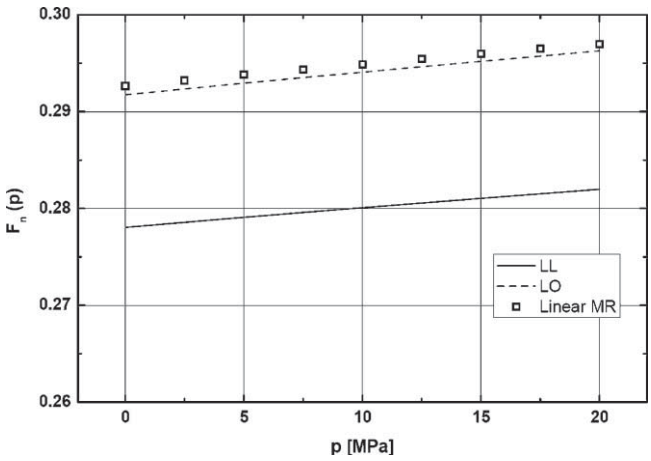

FIG. 11. Corresponding values of the function $F(n)$ as a function of the pressure for the binary mixture THN + C12 at 50 wt.%. The solid line represents the application of the LL formula (Eq. (9)) to the experimental data, while the dotted line represents the LO one (Eq. (10)). Open squares represent the right hand side of both equations and include the values of the molecular polarizability obtained by quantum calculations.

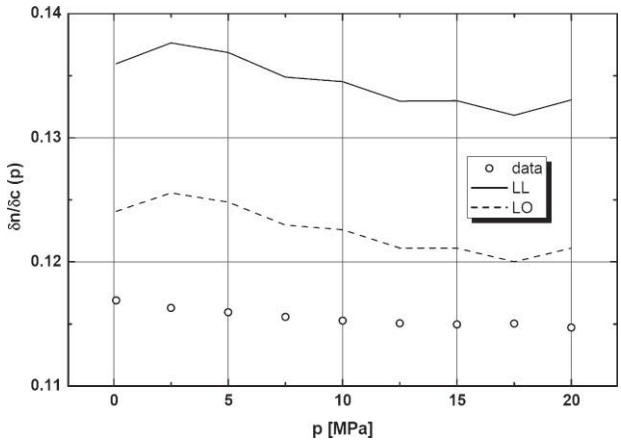

FIG. 12. Comparison between the experimental values of the concentration CF (empty circles) and theoretical predictions given by LL (continuous line) and LO (dashed line) approaches.

2. Comparison with theory

The density and mass expansion coefficient of the THN + C12 mixture were previously measured[35] in the pressure range from atmospheric pressure up to 20 MPa. For this reason the comparison between experimental data and theoretical predictions will be performed only up to this pressure level. The values of the density and the mass expansion coefficient together with the calculated polarizabilities and the molar masses ($M_1 = 132.2$ g mol^{-1} for THN, $M_2 = 170.34$ g mol^{-1} for C12) allowed us to perform a comparison between the experimental values of n and the concentration CF with the theoretical predictions provided by the LL and LO approaches, as by Eqs. (9)–(12). Figure 11 shows the results of the comparison between the experimental values for $F(n)$ (the left hand of Eqs. (9) and (10)) and the theoretical values provided by the right hand side of the same equations for the binary mixture THN + C12 at a mass fraction of 50%.

The calculated values fit well to those obtained from the LO formula, thus confirming the observations of Sengers and co-workers.[22] In Fig. 12, the experimental values of the concentration CF (empty circles) are compared with the theoretical predictions given by Eqs. (11) and (12), i.e., the theoretical values provided by the LL formula (continuous line) and by the LO formula (dashed line) with a linear mixing rule.

Again the predictions provided by the LO formula provide a better match with our experimental data points, even if, for the concentration CF that is a derived quantity, the discrepancy between experiment and theory is not negligible on the order of 6%. The discrepancy between experiment and the values given by LL formula is of the order of 14%.

V. CONCLUSIONS

In sight of future measurements of the Soret coefficients at high pressure for the mixture of THN + C12 at $c = 0.5$ and lacking of available data, our Mach-Zendher interferometer

has been modified to measure the concentration contrast factor $(\partial n/\partial c)_{P,T}$ at different pressures in the range between atmospheric pressure and 50 MPa. Measurements demonstrated an exponential decay in the concentration CF with pressure in the pressure range under investigation for this mixture. A comparison with theory required the calculation of the two molecules polarizabilities as a function of pressure. The comparison between our experimental results of n and the concentration CF with the results provided by Lorentz-Lorenz and Looyenga formulas extended to binaries with a linear mixing rule showed very good agreement with the Looyenga formula for the refractive index and a certain agreement with the deduced expression of concentration CF.

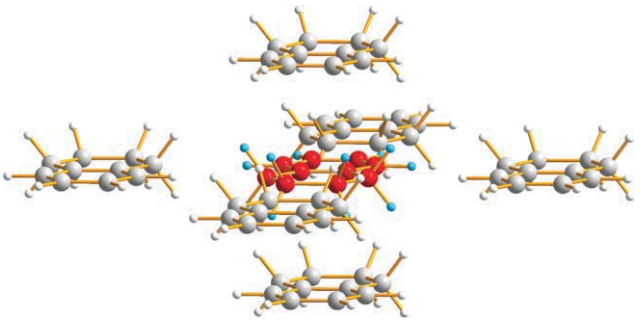

FIG. 13. Geometric equilibrium configuration for the six-embedded THN molecule for a given pressure.

ACKNOWLEDGMENTS

This work was financially supported by the European Space Agency and the PRES of Bordeaux. Ian Block is gratefully thanked for critically revising the paper. F.C. acknowledges present support from the European Union under Marie Curie funding, contract No. IEF-251131, DyNeFI Project.

APPENDIX: POLARIZABILITY QUANTUM CALCULATIONS

Ab initio calculations of (hyper)polarizabilities are nowadays of routine for molecular systems into gas phase, i.e., isolated systems.[36] Theoretical studies concerning many molecular systems developed with the help of analytical or numerical approaches is prolix in this field. So, it is not surprising to find theoretical data on systems studied in this work.[37] Nevertheless, pressure information is not available and models are generally not adapted to take into account this parameter. Automatic algorithms devoted to the calculation of local properties like individual polarizability under pressure must then be developed as detailed in the following.

Different configurations of the isolated and/or embedded THN and C12 fluids have been tested, the environmental effects such as pressure and interaction energies being key parameters in explaining the refractive index dependence, shown in the LL or LO formulas. *Ab initio* calculations were applied by using the 6-311+G** basis set.[38] The method used was the density functional theory (DFT), namely wB97XD (Ref. 39) including a long-range corrected hybrid density functional with damped atom-atom dispersion corrections. Optimized geometries, energies, and analytical first derivatives were obtained with the GAUSSIAN 09 package.[40] Zero-point energy, (an)harmonic frequencies,[41] dipole moments, mean static polarizability data,[42] molar volumes, and nonbonding orbital (NBO) atomic charges were also calculated. Basis-set superposition error was corrected with the use of the counterpoise method.

For each system, calculations were first carried out on up to six-embedded THN and C12 molecules in order to simulate the effect of pressure on global structures. Global relaxations on both the central and the lateral molecules were generated with the use of a Kshell/bash script devoted to the potential energy surfaces (PES) constructions and analysis. Three values of the pressure (0.1, 25, and 50 MPa) were taken into account corresponding to three different densities for each fluid (see Table I), and further generating three different values of the distance from the equilibrium state between six of the nearest neighbors and the central molecule as can be seen in the Fig. 13 for the THN molecule.

Eventually, the corresponding perturbed wave function of the central investigated system was then used to successfully solve the Schrödinger equation. The strategy used to calculate the electrical properties of the isolated wave-function under pressure effect is based on the polarizable solvent model (PCM) principle.[43] A molar model volume was used to calculate both refined relaxations and molecular densities. The analysis of correlations between PES and molar densities provides access to the conformation of the central system. The role of the environment was secondly taken into account in this system by using both cluster-conductor-like polarizable continuum model CPCM and SDM models.[44,45] In this approach, a continuous surface charge formalism ensures the continuity of the reaction field by expanding the apparent surface charge that builds up at the solute-environment interface in terms of spherical Gaussian functions located at each

TABLE I. THN and C12 density, polarizability, and Δd absolute variation distance between molecules from ground equilibrium state at atmospheric pressure as a function of the pressure.

	THN			C12		
Pressure (MPa)	Density (g cm^{-3})	Polarizability (a.u.)	Δd[a] (Å)	Density (g cm^{-3})	Polarizability (a.u.)	Δd[a] (Å)
0.1	0.9647	121.8350	0.000	0.7457	160.4777	0.000
25	0.9781	121.8387	0.014	0.7624	160.4967	0.017
50	0.9901	121.8419	0.028	0.7764	160.5119	0.033

[a]Distances are expressed between the centers of masses.

surface element in which the cavity surface is discretized. The solute radius (in Angstroms) was expressed in terms of molar density. Moreover, a dielectric constant of $\varepsilon = 1.911$ was chosen for the present study (similar to a non-polar solvent such as heptane). Finally, DFT analytical second derivatives were calculated for the determination of the three components α_{xx}, α_{yy}, and α_{zz}, as well as the mean polarizability $\bar{\alpha} = (\alpha_{xx} + \alpha_{yy} + \alpha_{zz})/3$ of the central molecule $\bar{\alpha}(P)$. Results are expressed in Table I in atomic unit (a.u.) corresponding to 0.148184×10^{-24} cm^{-3}.

The density of THN was measured with an HP 700 Anton-Paar densimeter, while the density of C12 was taken from handbooks. The dependence of the molecules polarizability until 50 MPa is weak. The values of the molecular polarizability of the two molecules we will take into account in the discussion are then: 121.84 ± 0.01 a.u. for the THN and 160.50 ± 0.02 a.u. for the C12 molecules.

Note that the theoretical model proposed in this work is unambiguous. It consists of directly taking into account the environmental effect (pressure) with the use of a polarizable continuum model (PCM). The computational choices made for the polarizability calculations are relative to the necessity to describe the polarization of the solute's electric field. So, both diffuse and not extended basis sets were used. At the same time, because of prime intermolecular interaction importance, the use of a dispersive DFT was also made. The absolute variations of the mean intermolecular distances from ground equilibrium state at atmospheric pressure are reported in Table I. As expected in the experimental range and because it concerns long range intermolecular phenomenon, very small variations are observed in those structural parameters. Nevertheless, if these variations seem very small reduce to a polarizability calculation, there are always significant and vary in the good direction regardless of the studied system.

As a simple test we have calculated the polarizability of the liquid toluene at 5 MPa. The calculated value is 91.88 a.u. For comparison the value calculated using Eq. (7) (LL formula) is 82.55 a.u. and using Eq. (8) (LO formula) we obtain 87.03 a.u. (we use the value of n and density of toluene at 5 MPa from literature). The deviation is of 11% from LL formula and 6% from LO formula. This allows us validating the quantum calculation procedure. Again we find a better agreement with LO formula.

[1] A. Mialdun and V. M. Shevtsova, Int. J. Heat Mass Transfer **51**, 3164 (2008).
[2] M. Giglio and A. Vendramini, Phys. Rev. Lett. **38**, 26 (1977).
[3] R. Piazza and A. Guarino, Phys. Rev. Lett. **88**, 208302-1 (2002).
[4] K. J. Zhang, M. E. Briggs, R. W. Gammon, and J. V. Sengers, J. Chem. Phys. **104**, 6881 (1996).
[5] P. Kolodner, H. Williams, and C. Moe, J. Chem. Phys. **88**, 6512 (1988).
[6] A. Vailati and M. Giglio, Nature (London) **390**, 262 (1997).
[7] A. Vailati and M. Giglio, Phys. Rev. Lett. **77**, 1484 (1996).
[8] D. Brogioli, A. Vailati, and M. Giglio, Phys. Rev. E **61**, R1 (2000).
[9] F. Croccolo, D. Brogioli, A. Vailati, M. Giglio, and D. S. Cannell, Ann. N.Y. Acad. Sci. **1077**, 365 (2006).
[10] F. Croccolo, D. Brogioli, A. Vailati, M. Giglio, and D. S. Cannell, Phys. Rev. E **76**, 41112 (2007).
[11] F. Croccolo, D. Brogioli, A. Vailati, M. Giglio, and D. S. Cannell, Appl. Opt. **45**, 2166 (2006).
[12] F. Croccolo, R. Cerbino, A. Vailati, and M. Giglio, in *Anomalous Fluctuation Phenomena in Complex Systems: Plasmas, Fluids, and Financial Markets*, edited by C. Riccardi and H. E. Roman (Research Signpost, Trivandrum, 2008).
[13] O. Ana, S. Ana, and A. Teklu, Appl. Opt. **49**, 86 (2010).
[14] H. C. van de Hulst, *Light Scattering by Small Particles* (Dover, New York, 1981).
[15] B. Chu, *Laser Light Scattering: Basic Principles and Practice* (Dover, New York, 2007).
[16] B. J. Berne and R. Pecora, *Dynamic Light Scattering: With Applications to Chemistry, Biology and Physics* (Dover, New York, 2000).
[17] P. N. Pusey and R. J. A. Tough, *Dynamic Light Scattering* (Plenum, New York, 1985).
[18] D. Brogioli, F. Croccolo, V. Cassina, D. Salerno, and F. Mantegazza, Opt. Express **16**, 20272 (2008).
[19] D. Brogioli, D. Salerno, V. Cassina, S. Sacanna, A. P. Philipse, F. Croccolo, and F. Mantegazza, Opt. Express **17**, 1222 (2009).
[20] D. Brogioli, D. Salerno, V. Cassina, and F. Mantegazza, Opt. Express **17**, 15431 (2009).
[21] F. Croccolo and D. Brogioli, Appl. Opt. **50**, 3419 (2011).
[22] W. B. Li, P. N. Segrè, R. W. Gammon, J. V. Sengers, and M. Lamvik, J. Chem. Phys. **101**, 5058 (1994).
[23] A. Becker, W. Köhler, and B. Müller, Ber. Bunsenges. Phys. Chem. **99**, 600 (1995).
[24] S. Van Vaerenbergh, A. Shapiro, G. Galliero, F. Montel, J. Legros, J. Caltagirone, J.-L. Daridon, and M. Z. Saghir, *Multicomponent Processes in Crudes* in European Space Agency Special Publication, Vol. 1290 (ESA Communications Production, Noordwijk, the Netherlands, 2005), pp. 202–213.
[25] F. Croccolo, H. Bataller, and G. Pijaudier-Cabot, AIP Conf. Proc. **1254**, 157 (2010).
[26] W. M. Rutherford and H. G. Drickamer, J. Chem. Phys. **22**, 1157 (1954).
[27] W. M. Rutherford and J. G. Roof, J. Phys. Chem. **63**, 1506 (1959).
[28] J. K. Platten, M. M. Bou-Ali, P. Costesèque, J. F. Dutrieux, W. Köhler, C. Leppla, S. Wiegand, and G. Wittko, Philos. Mag. **83**, 1965 (2003).
[29] T. Takagi and H. Teranishi, J. Chem. Eng. Data **27**, 16 (1982).
[30] A. J. Richard, J. Chem. Phys. **72**, 4063 (1980).
[31] A. H. Harvey, J. S. Gallagher, and J. M. H. Sengers, J. Phys. Chem. Ref. Data **27**, 761 (1998).
[32] G. Wittko and W. Köhler, Philos. Mag. **83**, 1973 (2003).
[33] H. A. Lorentz, *The Theory of Electrons* (Dover, New York, 1952).
[34] H. Looyenga, Mol. Phys. **9**, 501 (1965).
[35] H. Bataller, C. Miqueu, F. Plantier, J.-L. Daridon, T. J. Jaber, A. Abbasi, M. Z. Saghir, and M. M. Bou-Ali, J. Chem. Eng. Data **54**, 1710 (2009).
[36] A. Avramopoulos, M. G. Papadopoulos, and H. Reis, J. Phys. Chem. B **111**, 2546 (2007).
[37] A. M. Mkadmh, A. Hinchliffe, and F. M. Abu-Award, J. Mol. Struct.: THEOCHEM **901**, 9 (2007).
[38] J. D. Dill and J. A. Pople, J. Chem. Phys. **62**, 2921 (1975).
[39] J.-D. Chai and M. Head-Gordon, Phys. Chem. Chem. Phys. **10**, 6615 (2008).
[40] M. J. Frisch *et al.*, GAUSSIAN 09, Revision A.1, Gaussian, Inc., Wallingford, CT, 2009.
[41] D. Bégué, I. Baraille, P. A. Garrain, A. Dargelos, and T. Tassaing, J. Chem. Phys. **133**, 034102 (2010).
[42] M. Mérawa, D. Bégué, and A. Dargelos, J. Phys. Chem. A **107**, 9628 (2003).
[43] S. Miertuš, E. Scrocco, and J. Tomasi, Chem. Phys. **55**, 117 (1981).
[44] V. Barone and M. Cossi, J. Phys. Chem. A **102**, 1995 (1998).
[45] A. V. Marenich, C. J. Cramer, and D. G. Truhlar, J. Phys. Chem. B **113**, 6378 (2009).